

# TinyGLASS: Real-Time Self-Supervised In-Sensor Anomaly Detection

Pietro Bonazzi<sup>\*§</sup>, Rafael Sutter<sup>\*§</sup>, Luigi Capogrosso<sup>†</sup>, Mischa Buob<sup>‡</sup>, Michele Magno<sup>\*†</sup>

<sup>\*</sup>ETH Zurich, Zurich, Switzerland

<sup>†</sup>Interdisciplinary Transformation University of Austria, Linz, Austria

<sup>‡</sup>Swiss Engineering Partners AG, Zurich, Switzerland

**Abstract**—Anomaly detection plays a key role in industrial quality control, where defects must be identified despite the scarcity of labeled faulty samples. Recent self-supervised approaches, such as GLASS, learn normal visual patterns using only defect-free data and have shown strong performance on industrial benchmarks. However, their computational requirements limit the deployment on resource-constrained edge platforms, and even more so within in-sensor processing architectures. This work introduces TinyGLASS, a lightweight adaptation of the GLASS framework designed for real-time edge and in-sensor anomaly detection. The proposed architecture replaces the original WideResNet-50 backbone with a compact ResNet-18 and introduces deployment-based modifications that enable static graph tracing and INT8 quantization. We evaluated the proposed approach on the Sony IMX500 intelligent vision sensor, exploiting the in-sensor processor using the Sony Model Compression Toolkit. In addition to evaluating performance on the MVTec-AD benchmark, we investigate robustness to contaminated training data and introduce a custom industrial dataset, named MMS Dataset, for cross-device evaluation. Experimental results show that TinyGLASS achieves  $8.6\times$  parameter compression while maintaining competitive detection performance, reaching 94.2% image-level AUROC on MVTec-AD and operating at 20 FPS within the 8 MB memory constraints of the IMX500 platform. System profiling showcases low power consumption (4.0 mJ per inference), real-time end-to-end latency (20 FPS), and high energy efficiency (470 GMAC/J). Furthermore, the model demonstrates stable performance under moderate levels of training data contamination.

**Index Terms**—AIoT, Anomaly Detection, Self-Supervised Learning, TinyML, In-Sensor Computing.

## I. INTRODUCTION

In modern industrial manufacturing, visual inspection remains a crucial element of quality control. Although automation has advanced significantly, many inspection tasks are still performed by humans or by systems that require meticulously labeled data for training. This requirement poses a major limitation in real-world scenarios where labeled defect data are scarce, especially in settings characterized by a wide product variety and limited production volume, commonly referred to as *high-mix-low-volume* environments.

Recent developments in machine learning, particularly in anomaly detection, offer promising alternatives by enabling systems to learn normal visual patterns using only defect-free data [1], [2]. These approaches can detect irregularities

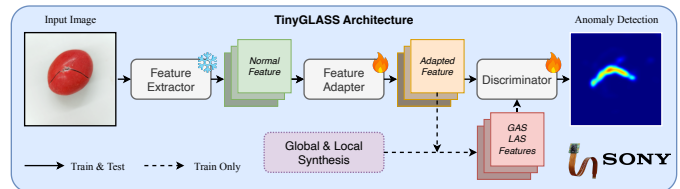


Figure 1. Schematic of the proposed TinyGLASS architecture for end-to-end anomaly detection in-sensor running at 20 FPS with only 5.41 MB of total memory.

without extensive defect annotation, making them attractive for industrial use [3].

However, small and medium enterprises with limited infrastructure and budgets often rely on low-cost edge computing devices for real-time quality control on their production lines [4], [5]. This dependence creates a gap between the high performance of advanced anomaly detection models and their practical deployment in real manufacturing environments [6].

To address this challenge, we present TinyGLASS (shown in Figure 1), a novel self-supervised anomaly detection model designed for in-sensor computing [7], [8]. Our main contributions are threefold.

First, we introduce TinyGLASS, a lightweight adaptation of the GLASS framework that replaces the original WideResNet-50 [9] backbone with a compact ResNet-18 [10] and incorporates deployment-aware modifications (static graph tracing and INT8 quantization) compatible with Sony’s Model Compression Toolkit [11]. Second, TinyGLASS achieves  $8.6\times$  parameter compression while providing competitive performance (94.2% image-level AUROC on MVTec-AD [12]) and runs at 20 FPS in only 5.41 MB on the novel Sony IMX500 intelligent vision sensor [13], representing the first demonstration of real-time in-sensor visual anomaly detection. Third, we thoroughly analyze robustness to contaminated training data and introduce a new custom industrial dataset (“MMS Dataset”) captured with both a high-resolution microscope and the IMX500 sensor, enabling cross-device evaluation.

## II. RELATED WORK

### A. Industrial Anomaly Detection

**Reconstruction-based methods** detect anomalies by analyzing the residual image before and after reconstruction under the assumption that a model trained only on normal data

The research was funded by the Swiss National Science Foundation (Grant 219943). <sup>§</sup>P. Bonazzi and R. Sutter contributed equally to this work.

will fail to accurately reconstruct abnormal regions. Early approaches used Autoencoders (AEs), Variational Autoencoders (VAEs) [14]. Other methods, such as [15], [16], frame anomaly detection as an inpainting problem in which image patches are randomly masked. However, they are heavily dependent on the quality of the reconstructed image. If anomalies share common patterns (*e.g.*, local edges) with normal data, or if the decoder is “too strong”, the defects may be reconstructed accurately, leading to small residual errors that fail to distinguish between normal and abnormal areas [15].

*Embedding-based methods* utilize pre-trained networks to extract features, and the extracted features are then used to learn normality. Memory bank methods, such as PatchCore [17] and PNI [18], represent normal features in an archive and detect anomalies using metric learning. Similarly, one-class classification methods, such as PANDA [19], map image features into a compact latent space where normal data is tightly clustered, allowing anomalies to be identified as points that fall outside this region. Other distribution-based approaches, such as PaDiM [20], model the normal state using Gaussian distributions at each pixel location. To better handle complex data, Normalizing Flow methods such as FastFlow [21], DifferNet [22], and CFLOW-AD [23] learn to transform normal feature distributions into a standard probability space. However, either computing the inverse of the covariance [20] or searching for the nearest neighbor in the memory bank [17] limits the feasibility of implementation and real-time performance in ultra-low-power devices.

*Synthesis-based methods* view the synthesis of anomalies as a form of data augmentation, creating “fake” defects on normal images to train a model to recognize what a deviation looks like [24], [25]. CutPaste [26] is the pioneer work in this area, generating anomalies by cutting a patch from one image and pasting it into another. DRAEM [27] improved this by using Perlin noise to simulate more realistic textures and training a network to locate and repair defects. Recently, SimpleNet [28] has achieved high accuracy using a simple discriminator to separate normal features from synthetic noise. GLASS [29] was proposed on top of SimpleNet, combining image-space corruptions with feature-space perturbations that improve weak defect detection.

### B. End-To-End Edge Vision

The design and deployment of neural networks for edge devices has attracted increasing attention in recent years [30]. Approaches typically balance model accuracy, computational efficiency, and hardware constraints and often rely on hardware-friendly operations, such as convolution micro-factorizations and lightweight network designs, which can be accelerated on embedded platforms.

In parallel, several works have evaluated deep learning models in a range of edge and embedded systems [31], [32]. For example, MCUNet [33] demonstrated end-to-end image classification on microcontrollers at  $\approx 10$  FPS, and TinyissimoYOLO [34] demonstrated an end-to-end object detection latency of 56 ms and 18 FPS [35].

More recently, in-sensor Artificial Intelligence (AI) platforms such as Sony IMX500 [13], [36] have enabled vision models to run directly on the image sensor, reducing system latency and energy consumption [32]. The usual applications of this platform span from general-purpose image segmentation [37], health monitoring [38], [39], and smart cities [40].

Despite these advances, end-to-end visual anomaly detection has not yet been demonstrated on in-sensor low-power edge platforms.

## III. METHODOLOGY

### A. Hardware Setup

The target deployment platform is the Sony IMX500 intelligent vision sensor [13], [36], a 12.3 MP CMOS sensor (approx.  $4056 \times 3040$  effective pixels,  $1.55 \mu\text{m}$  pixel size) that integrates an Image Signal Processing (ISP), a neural network accelerator, and on-chip AI inference capabilities. This enables the execution of quantized deep neural networks directly on the sensor, producing metadata or anomaly scores rather than full images, thereby reducing bandwidth, latency, and energy consumption in edge applications [8], [32]. In recent years, the IMX500 has been integrated via the Raspberry Pi AI Camera [41], which connects to a Raspberry Pi 5 via the standard MIPI CSI-2 interface. Network inference produces patch-level anomaly heatmaps directly from the sensor, while the final image-level decisions are aggregated on the host (Raspberry Pi) if required. This setup enables in-sensor real-time anomaly detection.

### B. TinyGLASS Architecture

TinyGLASS is an efficient anomaly detection architecture, adapted from GLASS [29], to enable deployment on resource-constrained embedded platforms, such as the Sony IMX500 intelligent vision sensor.

While some components of the original GLASS pipeline remain effective on GPU-based platforms, they are not compatible with the constraints imposed by embedded proxy tracking and quantization frameworks used for low-power processing. The adaptations proposed here preserve the core anomaly detection capabilities while enabling efficient real-time execution on resource-constrained hardware.

First, the original GLASS architecture is based on a Wide-ResNet-50 [9] backbone that produces 1536-dimensional embeddings from concatenated level-2 and level-3 features. To reduce memory footprint and computational demands while preserving the multi-scale feature fusion strategy, we replace this backbone with ResNet-18 [10], producing 384-dimensional concatenated embeddings from the corresponding layers. Intermediate feature extraction, previously performed via PyTorch hooks, is replaced by a modified forward pass that directly returns only the required level-2 and level-3 layers. This change enables the pruning of unused components and ensures compatibility with the static graph tracing required for hardware-aware quantization [11].

Dynamic tensor reshaping and unsupported operations are also eliminated to satisfy strict operator constraints during

tracing, which replaces tensors with symbolic proxies and invokes the `forward` method under static shapes. In addition, the input path of the discriminator, originally involving a `flatten` operation followed by linear and convolutional layers, introduces dynamic shapes that violate these constraints. We resolve this by maintaining 4D tensor representations end-to-end, enabling standard `Conv2D` operations throughout. Furthermore, the tuple returns between modules are replaced with single-tensor outputs; specifically, the interpolated features of layer-2 and layer-3 of the backbone are concatenated into a unified tensor.

The final network output is a single tensor of patch-level anomaly scores (*i.e.*, a heatmap), while image-level scores are computed on the host side. To have an in-sensor evaluation on IMX500’s vision sensors [13], [36], compression is performed using Sony’s Model Compression Toolkit [11], with both weights and activations quantized to INT8.

In terms of model complexity, the ResNet-18 backbone used in TinyGLASS contains 14.6 M parameters when fully instantiated. However, only the layers up to `layer3` are executed during inference, resulting in an effective backbone size of 2.78 M parameters. The discriminator head, identical to that of GLASS, adds an additional 67.5 K parameters. Including the remaining intermediate components (*e.g.*, the PatchMaker), the total number of parameters actively used at inference is approximately 2.9 M. Compared to 24.9 M for the corresponding GLASS configuration based on WideResNet-50, this yields an effective compression ratio of  $8.6\times$ .

### C. Training Objective & Implementation Details

As illustrated in Figure 1, TinyGLASS leverages two complementary feature representations, namely the Global Anomaly Score (GAS) and the Local Anomaly Score (LAS) proposed in [29]. GAS captures coarse, image-level deviations by aggregating global contextual information, while LAS focuses on fine-grained, spatially localized discrepancies that are critical for detecting small or subtle anomalies.

The training objective combines two complementary loss terms to effectively distinguish anomalous samples from normal ones:

$$\mathcal{L}_{\text{total}} = \mathcal{L}_{\text{BCE}} + \mathcal{L}_{\text{focal}}, \quad (1)$$

where  $\mathcal{L}_{\text{BCE}}$  is the Binary Cross-Entropy loss [42] used for discriminator training, and  $\mathcal{L}_{\text{focal}}$  is the Focal Loss [43] applied to handle the class imbalance between normal and defective regions.

Our training protocol follows the standard unsupervised anomaly detection framework using only good samples during training, unless otherwise stated. Patch-level anomaly scores are aggregated to produce final image-level predictions. Data augmentation includes random rotations, translations, color jittering, and horizontal/vertical flips, applied with probability 0.5 to increase the model’s robustness.

The model is trained using AdamW optimizer [44] with a learning rate of  $10^{-4}$  for the feature extraction components and  $2 \times 10^{-4}$  for the discriminator. We train on three NVIDIA

Table I  
PER-CLASS SAMPLE DISTRIBUTION IN THE CUSTOM MMS DATASET  
ACROSS THE TWO CAMERA SETUPS.

Camera Category	Microscope		IMX500	
	Train	Test+Val	Train	Test+Val
Normal / Good	166	42	184	55
Crack-hole	0	18	0	28
Scratch	0	39	0	42
Half	0	14	0	14
Defective (all types)	<b>0</b>	<b>71</b>	<b>0</b>	<b>84</b>
<b>Total</b>	<b>166</b>	<b>113</b>	<b>184</b>	<b>139</b>

RTX A6000 for a maximum of 200 epochs, with a batch size of 8. The best model is selected on the basis of the image-level AUROC performance.

### D. Datasets

We evaluate the proposed TinyGLASS model on two complementary datasets: *i)* our newly introduced *MMS dataset*, which captures real-world industrial micro-component defects using both a high-resolution microscope and the target Sony IMX500 sensor, enabling direct assessment of domain transfer and edge-deployment feasibility; and *ii)* the widely used MVTec-AD benchmark [12], a standard industrial anomaly detection dataset that allows comparison with prior methods and controlled experiments on training-set contamination to simulate realistic imperfect data collection scenarios.

**MMS dataset.** To evaluate domain transfer and real-world applicability, we introduce the custom MMS dataset, collected under controlled laboratory conditions. The images were captured using a stereo zoom microscope (RYF AG) with a trinocular head mounted on an articulated boom arm. A high-resolution camera stream was monitored in real time, enabling precise adjustment of exposure, gain, contrast, and measurement overlays. The samples were recorded with fixed magnification and controlled illumination to reduce acquisition variance. To further study domain shift, a subset of images was also captured using the Sony IMX500 intelligent vision sensor [13], [36], which allowed future cross-device evaluation and facilitated experiments targeting edge deployment. The final dataset comprises four defect categories, *i.e.*, *crack-hole*, *scratch*, *half*, and *normal*, covering structural and surface-level anomalies.

In Table I, we provide statistics for two camera setups: the high-resolution microscope camera used for primary experiments and the IMX500 camera for additional domain-transfer evaluation. Figure 2 shows representative examples and illustrates the acquisition setup.

**MVTec-AD dataset.** The MVTec-AD benchmark [12] provides defect-free training images and pixel-annotated anomalous test samples across 15 industrial categories. We resized the input images to  $256 \times 256$  pixels and normalized them using ImageNet statistics [45] before processing them by the network. To simulate realistic industrial conditions where

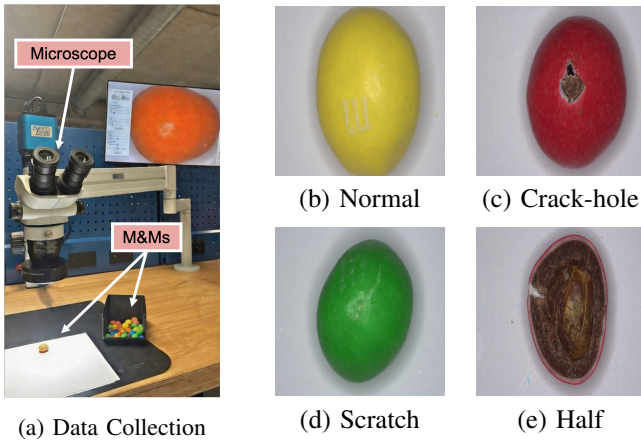


Figure 2. MMS Dataset. Left: stereo microscope acquisition setup. Right: representative samples of the four classes.

Table II  
COMPARISON OF GLASS AND TINYGLASS ON MVTEC-AD (MEAN RESULTS). TINYGLASS ACHIEVES 8.6 $\times$  PARAMETER COMPRESSION WITH A 4.9% I-AUROC DROP.

Model	Format	Params	AUROC (%)	
			Image	Pixel
GLASS [29]	float-32	24.9 M	99.1	98.3
TinyGLASS (ours)	float-32	2.9 M	94.6	92.9
TinyGLASS (ours)	int-8	-	94.2	90.9

normal-only training data may be contaminated, we inject anomalous samples into the training set for the carpet category. We vary the contamination ratio between 5% and 30%, sampling defective images from the held-out subsets. This setting enables controlled analysis of robustness under imperfect supervision.

#### IV. EXPERIMENTAL RESULTS

We evaluate TinyGLASS in terms of detection accuracy and deployment efficiency. First, we compare TinyGLASS with the original GLASS model on the MVTEC-AD benchmark. Next, we analyze the robustness to training-set contamination. Finally, we report system-level performance of the model deployed on the target hardware platform.

Table II reports the mean performance on MVTEC-AD. TinyGLASS achieves 94.2% image-level AUROC (I-AUROC) and 90.9% pixel-level AUROC (P-AUROC), corresponding to drops of 4.9% and 7.4% compared to GLASS. On the custom MMS dataset, the model reaches 88.9% I-AUROC when trained and tested on the microscope images.

To evaluate robustness to training set contamination, anomalous samples are injected into the training set at rates of 0%, 5%, 10%, 20%, and 30%. I-AUROC and P-AUROC are reported in Figure 3. On MVTEC-AD (only *carpet*), I-AUROC decreases from 95.6% at 0% contamination to 88.3% at 30%. On MMS, I-AUROC decreases from 88.9% to 84.2% in the same range. P-AUROC drops from 99.2% to 80.8% on MVTEC-AD carpet over the same contamination range.

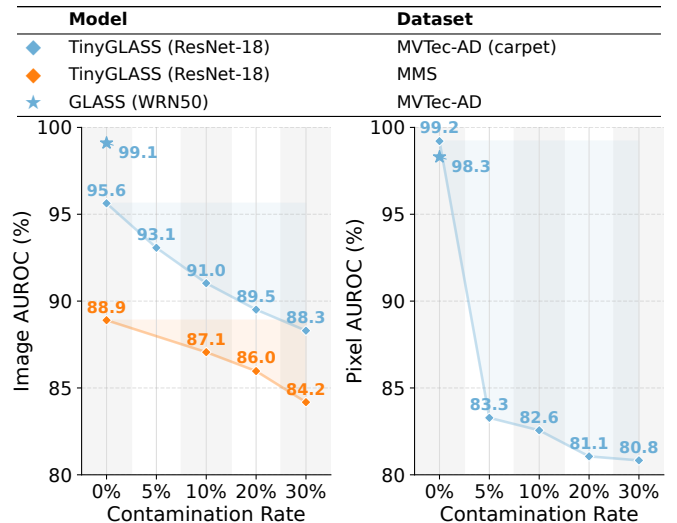


Figure 3. Effect of training-set contamination on TinyGLASS (ResNet-18) evaluated on MVTEC-AD (*carpet*) and MMS. I-AUROC (left) and P-AUROC (right) are shown for contamination rates ranging from 0 to 30%. GLASS (WideResNet-50) on full MVTEC-AD is shown as a reference at 99.2%.

Finally, we evaluate the TinyGLASS system deployed on the target edge platform. In terms of runtime performance on the Sony IMX500, the system achieves approximately 20 FPS during inference. Each inference requires only 1.88 G Multiply-Accumulate Operations (MACs) for  $256 \times 256$  input images (1.844 G in the backbone, 0.016 G in PatchMaker, and 0.017 G in the discriminator). This corresponds to an effective throughput of 37.6 GMAC/s, an efficiency of 470 GMAC/J, and an energy consumption of 4.0 mJ per inference, among the lowest reported for the in-sensor anomaly detection models deployed.

#### V. CONCLUSION & FUTURE WORK

This work presented TinyGLASS, a lightweight self-supervised anomaly detection framework designed for deployment on resource-constrained edge vision platforms, including in-sensor processors. Experimental results on the MVTEC-AD benchmark demonstrate that TinyGLASS achieves substantial model compression while maintaining competitive detection performance. Specifically, TinyGLASS reduces the parameter count by 8.6 $\times$ , while still achieving 94.2% I-AUROC. System-level evaluation shows that the quantized model fits within the 8 MB memory constraint of the target platform and achieves real-time inference at approximately 20 FPS on the novel Sony IMX-500. In addition, we evaluated robustness to contaminated training data and introduced a custom dataset for domain-transfer analysis. The results indicate that TinyGLASS maintains stable performance under moderate levels of label misclassification. Future work could explore further improvements in model robustness and efficiency, including lightweight backbone architectures [46]–[48], broader validation across industrial inspection scenarios [49], and investigate explainable anomaly detection methods that provide interpretable localization and defect characterization.

## REFERENCES

- [1] H. Hojjati *et al.*, “Self-supervised anomaly detection in computer vision and beyond: A survey and outlook,” *Neural Networks*, vol. 172, p. 106106, 2024.
- [2] Z. Li *et al.*, “A survey of deep learning for industrial visual anomaly detection,” *Artificial Intelligence Review*, vol. 58, no. 9, 2025.
- [3] J. Liu *et al.*, “Deep Industrial Image Anomaly Detection: A Survey,” *Machine Intelligence Research*, vol. 21, no. 1, pp. 104–135, 2024.
- [4] M. Antonini *et al.*, “An Adaptable and Unsupervised TinyML Anomaly Detection System for Extreme Industrial Environments,” *Sensors*, vol. 23, no. 4, p. 2344, 2023.
- [5] U. Khan *et al.*, “KairosAD: A SAM-Based Model for Industrial Anomaly Detection on Embedded Devices,” in *23rd International Conference on Image Analysis and Processing (ICIAP)*, 2025.
- [6] M. Barusco *et al.*, “PaSTe: Improving the Efficiency of Visual Anomaly Detection at the Edge,” in *IEEE/CVF Conference on Computer Vision and Pattern Recognition Workshops (CVPRW)*, 2025.
- [7] D. P. Pau *et al.*, “Reviewing progresses on In-Sensor AI Computing,” *Microprocessors and Microsystems*, p. 105156, 2025.
- [8] L. Capogrosso *et al.*, “Performance Analysis of Edge and In-Sensor AI Processors: A Comparative Review,” *arXiv preprint arXiv:2603.08725*, 2026.
- [9] S. Zagoruyko *et al.*, “Wide Residual Networks,” in *British Machine Vision Conference (BMVC)*, 2016.
- [10] K. He *et al.*, “Deep Residual Learning for Image Recognition,” in *IEEE Conference on Computer Vision and Pattern Recognition (CVPR)*, 2016.
- [11] Sony Semiconductor Solutions, “Model Compression Toolkit (MCT),” <https://github.com/SonySemiconductorSolutions/mct-model-optimization>, accessed: 2026-03-05.
- [12] P. Bergmann *et al.*, “MVTEC AD – A Comprehensive Real-World Dataset for Unsupervised Anomaly Detection,” in *IEEE/CVF Conference on Computer Vision and Pattern Recognition (CVPR)*, 2019.
- [13] Sony Semiconductor Solutions, “IMX500,” <https://developer.sony.com/imx500>, accessed: 2025-11-30.
- [14] D. Gong *et al.*, “Memorizing Normality to Detect Anomaly: Memory-Augmented Deep Autoencoder for Unsupervised Anomaly Detection,” in *IEEE/CVF International Conference on Computer Vision (ICCV)*, 2019.
- [15] V. Zavrtanik *et al.*, “Reconstruction by inpainting for visual anomaly detection,” *Pattern Recognition*, vol. 112, p. 107706, 2021.
- [16] N.-C. Ristea *et al.*, “Self-Supervised Predictive Convolutional Attentive Block for Anomaly Detection,” in *IEEE/CVF Conference on Computer Vision and Pattern Recognition (CVPR)*, 2022.
- [17] K. Roth *et al.*, “Towards Total Recall in Industrial Anomaly Detection,” in *IEEE/CVF Conference on Computer Vision and Pattern Recognition (CVPR)*, 2022.
- [18] J. Bae *et al.*, “Pni : Industrial anomaly detection using position and neighborhood information,” in *IEEE/CVF International Conference on Computer Vision (ICCV)*, 2023.
- [19] T. Reiss *et al.*, “PANDA: Adapting Pretrained Features for Anomaly Detection and Segmentation,” in *IEEE/CVF Conference on Computer Vision and Pattern Recognition (CVPR)*, 2021.
- [20] T. Defard *et al.*, “PaDiM: A Patch Distribution Modeling Framework for Anomaly Detection and Localization,” in *25th International Conference on Pattern Recognition Workshops (ICPRW)*, 2021.
- [21] J. Yu *et al.*, “FastFlow: Unsupervised Anomaly Detection and Localization via 2D Normalizing Flows,” *arXiv preprint arXiv:2111.07677*, 2021.
- [22] M. Rudolph *et al.*, “Same Same but DifferNet: Semi-Supervised Defect Detection With Normalizing Flows,” in *IEEE/CVF Winter Conference on Applications of Computer Vision (WACV)*, 2021.
- [23] D. Gudovskiy *et al.*, “CFLOW-AD: Real-Time Unsupervised Anomaly Detection with Localization via Conditional Normalizing Flows,” in *IEEE/CVF Winter Conference on Applications of Computer Vision (WACV)*, 2022.
- [24] L. Capogrosso *et al.*, “Diffusion-Based Image Generation for In-Distribution Data Augmentation in Surface Defect Detection,” in *19th International Conference on Computer Vision Theory and Applications (VISAPP)*, 2024.
- [25] F. Girella *et al.*, “Leveraging Latent Diffusion Models for Training-Free in-Distribution Data Augmentation for Surface Defect Detection,” in *International Conference on Content-Based Multimedia Indexing (CBMI)*, 2024.
- [26] C.-L. Li *et al.*, “CutPaste: Self-Supervised Learning for Anomaly Detection and Localization,” in *IEEE/CVF Conference on Computer Vision and Pattern Recognition (CVPR)*, 2021.
- [27] V. Zavrtanik *et al.*, “DRAEM - A Discriminatively Trained Reconstruction Embedding for Surface Anomaly Detection,” in *International Conference on Computer Vision (ICCV)*, 2021.
- [28] Z. Liu *et al.*, “SimpleNet: A Simple Network for Image Anomaly Detection and Localization,” in *Conference on Computer Vision and Pattern Recognition (CVPR)*, 2023.
- [29] W. Chen *et al.*, “A Unified Anomaly Synthesis Strategy with Gradient Ascent for Industrial Anomaly Detection and Localization,” in *European Conference on Computer Vision (ECCV)*, 2024.
- [30] L. Capogrosso *et al.*, “A Machine Learning-Oriented Survey on Tiny Machine Learning,” *IEEE Access*, vol. 12, pp. 23 406–23 426, 2024.
- [31] M. Giordano *et al.*, “Survey and Comparison of Milliwatts Micro controllers for Tiny Machine Learning at the Edge,” in *4th International Conference on Artificial Intelligence Circuits and Systems (AICAS)*, 2022.
- [32] P. Bonazzi *et al.*, “TinyTracker: Ultra-Fast and Ultra-Low-Power Edge Vision In-Sensor for Gaze Estimation,” *IEEE Sensors*, 2023.
- [33] J. Lin *et al.*, “MCUNet: Tiny Deep Learning on IoT Devices,” in *Advances in Neural Information Processing Systems (NeurIPS)*, 2020.
- [34] J. Moosmann *et al.*, “TinyissimoYOLO: A Quantized, Low-Memory Footprint, TinyML Object Detection Network for Low Power Micro-controllers,” in *5th International Conference on Artificial Intelligence Circuits and Systems (AICAS)*, 2023.
- [35] J. Moosmann *et al.*, “Ultra-Efficient On-Device Object Detection on AI-Integrated Smart Glasses with TinyissimoYOLO,” in *European Conference on Computer Vision (ECCV) Workshops*, 2024.
- [36] R. Eki *et al.*, “9.6 A 1/2.3inch 12.3Mpixel with On-Chip 4.97TOPS/W CNN Processor Back-Illuminated Stacked CMOS Image Sensor,” in *IEEE International Solid-State Circuits Conference (ISSCC)*, 2021.
- [37] P. Bonazzi *et al.*, “PicoSAM2: Low-Latency Segmentation In-Sensor for Edge Vision Applications,” in *IEEE SENSORS*, 2025.
- [38] Q. Tong *et al.*, “Edge AI-enabled chicken health detection based on enhanced FCOS-Lite and knowledge distillation,” *Computers and Electronics in Agriculture*, vol. 226, p. 109432, 2024.
- [39] P. Bonazzi *et al.*, “Q-Segment: Segmenting Images In-Sensor for Vessel-Based Medical Diagnosis,” in *IEEE 6th International Conference on AI Circuits and Systems (AICAS)*, 2024.
- [40] T. Cui *et al.*, “Pedestrian Warning: Intelligent Vision Sensor vs. Edge AI with LTE C-V2X in a Smart City,” in *IEEE 99th Vehicular Technology Conference (VTC2024-Spring)*, 2024.
- [41] Raspberry Pi Documentation, “The Raspberry Pi AI Camera,” <https://www.raspberrypi.com/documentation/accessories/ai-camera.html>, accessed: 2026-03-05.
- [42] S. J. Prince, *Understanding Deep Learning*. MIT press, 2023.
- [43] T.-Y. Lin *et al.*, “Focal Loss for Dense Object Detection,” in *IEEE International Conference on Computer Vision (ICCV)*, 2017.
- [44] I. Loshchilov *et al.*, “Decoupled Weight Decay Regularization,” in *International Conference on Learning Representations*, 2019.
- [45] J. Deng *et al.*, “ImageNet: A Large-Scale Hierarchical Image Database,” in *IEEE Conference on Computer Vision and Pattern Recognition (CVPR)*, 2009.
- [46] F. N. Iandola *et al.*, “SqueezeNet: AlexNet-level accuracy with 50x fewer parameters and < 0.5 MB model size,” in *International Conference on Learning Representations (ICLR)*, 2017.
- [47] A. Howard *et al.*, “Searching for MobileNetV3,” in *International Conference on Computer Vision (ICCV)*, 2019.
- [48] M. Tan *et al.*, “EfficientNet: Rethinking Model Scaling for Convolutional Neural Networks,” in *International Conference on Machine Learning (ICML)*, 2019.
- [49] Y. Zou *et al.*, “SPot-the-Difference Self-supervised Pre-training for Anomaly Detection and Segmentation,” in *European Conference on Computer Vision (ECCV)*, 2022.